PHYSICAL REVIEW E **91**, 010701(R) (2015)

Seizures, refractory status epilepticus, and depolarization block as endogenous brain activities

Kenza El Houssaini, Anton I. Ivanov, Christophe Bernard, and Viktor K. Jirsa*
Aix Marseille Université, Inserm, INS UMR_S 1106, 13005, Marseille, France
(Received 11 September 2014; published 8 January 2015)

Epilepsy, refractory status epilepticus, and depolarization block are pathological brain activities whose mechanisms are poorly understood. Using a generic mathematical model of seizure activity, we show that these activities coexist under certain conditions spanning the range of possible brain activities. We perform a detailed bifurcation analysis and predict strategies to escape from some of the pathological states. Experimental results using rodent data provide support of the model, highlighting the concept that these pathological activities belong to the endogenous repertoire of brain activities.

DOI: 10.1103/PhysRevE.91.010701 PACS number(s): 87.19.ll, 87.19.xm, 05.45.−a

Introduction. Pathological discharges in neural tissue occur on various time scales ranging from milliseconds to minutes and are typically considered separate physiological events, characterized by their different patterns of neuronal activities [1] and ionic changes [2–5]. Epilepsy is defined by the occurrence of recurrent seizures characterized by an onset and offset. Seizures show fast discharges (10-ms time scale) and evolve slowly, lasting from seconds to minutes. A seizure can sometimes evolve into so-called refractory status epilepticus (RSE), that is, a seizure with continuous discharges, which is very difficult to treat [6], often leading to patient death. Another pathological discharge is known as spreading depression, which may occur during migraine and some seizures [7,8] and is characterized by a slowly propagating depolarization wave, during which neurons go into depolarization block (DB), followed by a shutdown of brain activity [7]. Depolarization block is a physiological state, in which the neuronal membrane is depolarized, but action potentials cannot be triggered. The mechanisms underlying the genesis of all these pathological activities remain unknown. Recent accumulating evidence supports the view that these different pathological discharges may be described in a common framework [2,3,9]. Here we address this question from a theoretical perspective via neural mass modeling. Through numerical and mathematical analyses we determine the conditions under which normal brain activities, seizures, RSE, and DB coexist and how transitions from one state to another can occur. We then provide supporting evidence of the theoretical predictions in the intact immature hippocampus as an experimental model, demonstrate how RSE can be stopped, and lay out an experimental strategy for model validation.

The Epileptor. Neural population models, also called neural mass models, describe seizures and their onset and offset via bifurcations [10–12]. Jirsa *et al.* classified seizures systematically into classes of onset and offset bifurcation pairs [13]. The most prominent class of seizures is characterized by the saddle-node/homoclinic bifurcation pair. The canonical model associated with this pairing is the square-wave burster. Additional degrees of freedom linked to inhibitory couplings between gamma-aminobutyric acid (GABA) and glutamatergic neurons are due to a second subsystem exhibiting a saddle-node/invariant-circle bifurcation pair generating interictal spikes and various details of seizure evolution during the ictal phase. A slow permittivity variable accounts for, presumably predominantly, extracellular effects related to energy consumption and oxygen. The complete model, referred to as the Epileptor, consists of five coupled nonlinear differential-integral equations, comprising the first subsystem with two state variables x_1 and y_1 responsible for generating fast discharges, a second subsystem with two state variables x_2 and y_2 generating sharp-wave events, and a slow state variable z, which drives the dynamics of the Epileptor [13]. The following equations generate seizure-like events (SLEs):

$$\dot{x}_1 = y_1 - f_1(x_1,x_2) - z + I_{\text{ext}_1}, \tag{1}$$

$$\dot{y}_1 = c_1 - d_1 x_1^2 - y_1, \tag{2}$$

$$\dot{z} = \begin{cases} r[s(x_1 - x_0) - z - 0.1z^7] & \text{if} \quad z < 0 \\ r[s(x_1 - x_0) - z] & \text{if} \quad z \geqslant 0, \end{cases} \tag{3}$$

$$\dot{x}_2 = -y_2 + x_2 - x_2^3 + I_{\text{ext}_2} + 2g - 0.3(z - 3.5), \tag{4}$$

$$\dot{y}_2 = [-y_2 + f_2(x_2)]/\tau_2, \tag{5}$$

where

$$f_1(x_1,x_2) = \begin{cases} a_1 x_1^3 - b_1 x_1^2 & \text{if} \quad x_1 < 0 \\ -[m - x_2 + 0.6(z-4)^2]x_1 & \text{if} \quad x_1 \geqslant 0, \end{cases}$$

$$f_2(x_2) = \begin{cases} 0 & \text{if} \quad x_2 < -0.25 \\ a_2(x_2 + 0.25) & \text{if} \quad x_2 \geqslant -0.25, \end{cases}$$

$$g(x_1) = \int_{t_0}^{t} e^{-\gamma(t-\tau)} d\tau,$$

with the parameters a_1=1, b_1=3, c_1=1, d_1=5, I_{ext_1}=3.1, $m = 0, a_2 = 6, \tau_2 = 10, I_{\text{ext}_2} = 0.45, \gamma = 0.01, r = 0.000\,35$, $s = 4$, and $x_0 = -1.6$. Time series of the whole system and the various subsystems are plotted in Fig. 1(a), exhibiting the major elements of a SLE. The trajectory in state space of subsystem 1 and the z variable is plotted in Fig. 1(b). All stochastic simulations are performed with linearly additive Gaussian white noise with zero mean and a variance of 0.0025 using the Euler-Maruyama method.

Bifurcation diagram. Using analytic and numerical continuation, we derive the (z,x_1) bifurcation diagram of the Epileptor in Fig. 2. The bifurcation curve is a Z-shaped curve known from fast-slow subsystems [14]. The lower branch

*Author to whom correspondence should be addressed: viktor.jirsa@univ-amu.fr

 ©2015 American Physical Society

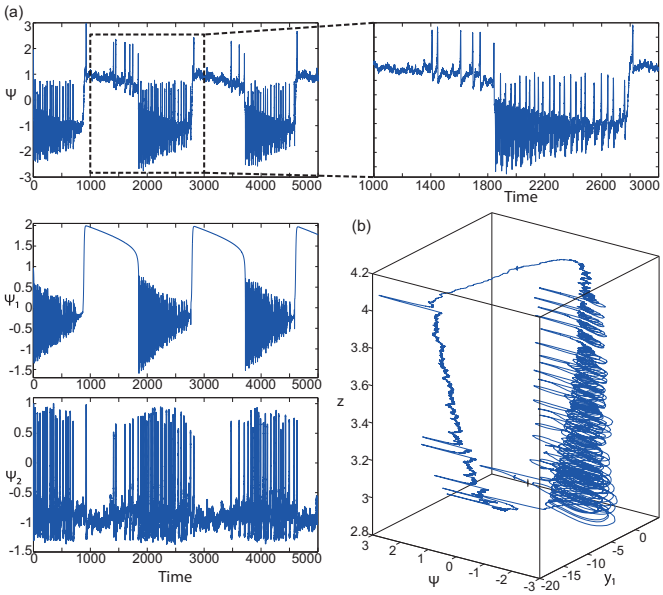

FIG. 1. (Color online) Seizure dynamics. (a) Time series of the Epileptor model (its enlarged view is shown on the right). The first (middle) and second (bottom) subsystems are plotted showing the principal components of a seizure-like event, that is, an interictal period with no spikes, emergence of preictal spikes, ictal onset, seizure evolution, and emergence of sharp-wave events towards ictal offset. Here ψ, ψ_1, and ψ_2 correspond to $-x_1 + x_2$, x_1, and x_2, respectively. (b) Trajectory of the whole system sketched in the (y_1, ψ, z) phase space. Seizure offset and ictal onset emerge through the z evolution. Here all simulations were performed with Gaussian white noise using the Euler-Mayurama method.

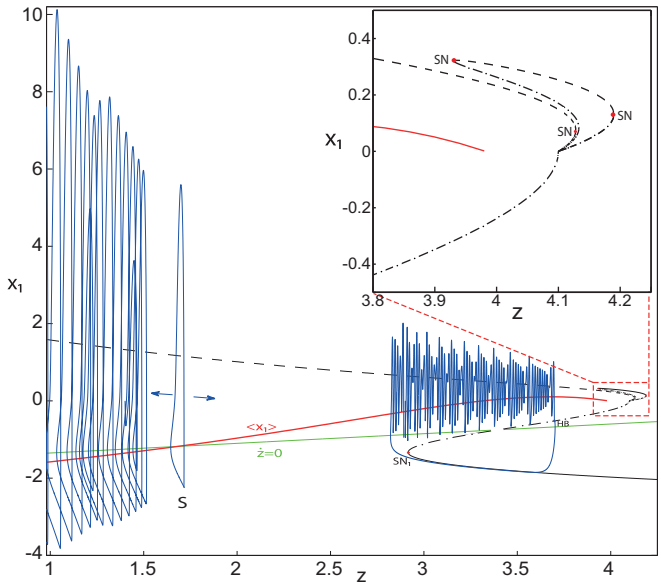

FIG. 2. (Color online) Epileptor model bifurcation diagram with respect to the slow variable z ($m = 0.5$). The upper (dashed line), lower (solid line), and middle (dash-dotted line) branches of the Z-shaped curve consist of unstable focus, stable nodes, and saddles respectively. Above, lower (dash-dotted line) and upper (dashed line) branches corresponding to saddles and unstable focus, respectively, collide in a saddle-node bifurcation (SN). The inset is their enlarged view. A SLE occurs with a saddle-node/homoclinic bifurcation pair. A saddle S periodic orbit separates the SLE attractor (right) and a stable periodic orbit LC (to the left; the final orbit is not shown). Characteristic trajectories are plotted on both sides of the separatrix S defining two basins of attraction (indicated by arrows).

comprises stable nodes (the non-ictal state) and the upper branch an unstable focus (the ictal state). The middle branch consists of saddle points. With decreasing z, the lower and middle branches collide at a saddle-node bifurcation SN_1. Two branches above the Z curve (see the inset) comprising an unstable focus (dashed line) and saddles (dash-dotted line) collide in a SN bifurcation as z decreases. We identify two important bifurcations of the Epileptor dynamics. The first bifurcation that results in a transition from offset to onset states occurs through a saddle-node bifurcation SN_1. The second one that results in a transition from onset to offset states occurs through a homoclinic bifurcation (HB). The whole system is bistable on $[SN_1, HB]$. The equilibrium points of the Epileptor model lie on the intersection of the z nullcline ($\dot{z} = 0$) with the bifurcation diagram curves (Fig. 2). We set $x_0 = -1.6$, the z nullcline is at the middle branch, and then the equilibrum point is a saddle, thereby allowing the transitions between onset and offset states, leading to a recurrence of SLEs. When a trajectory is at a lower branch of the Z curve, the stable node disappears as z decreases via a saddle-node bifurcation and the whole system switches to the Z upper branch exhibiting an oscillatory (ictal) solution, which terminates in a HB bifurcation. We trace the limit cycle averaged curve $\langle x_1 \rangle$ for each z value intersecting the z nullcline at two points consisting of stable and saddle S periodic orbits. Towards the left-hand side in Fig. 2 we plot the trajectory as it transients towards a stable limit cycle (the latter is not shown). The saddle periodic orbit separates the basin of attraction of the stable periodic orbit (left) and the basin of attraction of the SLE (right).

Coexistence of seizures, refractory status epilepticus, depolarization block, and normal state. Pathological activities may coexist within the normal brain or may require altered neuronal circuits (e.g., a brain lesion, a gene mutation, etc.) to occur. To explore this issue theoretically, we establish coexistence by varying the initial conditions of the Epileptor over a large state space region and parameter regime. Relevant parameters are x_0 and m, which are linked to the degree of epileptogenicity and fast discharges [13,15]. The search reveals the existence of a so far unknown stable periodic solution with large amplitude and fast-slow invariant cycle. The new stable limit cycle (LC) and the original SLE attractor coexist and are separated by a saddle periodic orbit [Fig. 3(a)]; below a critical value, z decays to below a baseline shift to converge to the LC. Characteristic time series are shown in Fig. 3(b) for SLE and in Fig. 3(c) for the LC. The latter LC is composed of a fast and slow manifold and thus displays fast-slow cyclic behavior, which is reminiscent of RSE [16]. With decreasing m, the fast manifold of the SLE attractor in the upper part of Fig. 3(a) collapses to a point that traces out a line under slow z evolution. Thus the SLE attractor reduces to a periodic switch between two slow manifolds [Figs. 4(a) and 4(b)], which are indicated by segment numbers 1 for DB and 3 for the normal state (NS).

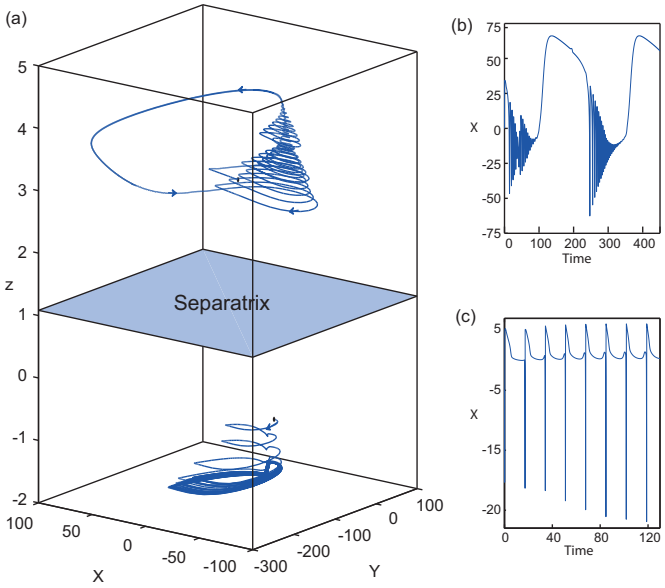

FIG. 3. (Color online) (a) Coexistence of seizure-like events and refractory status epilepticus. The simulations are performed without noise. Seizure-like events and a stable limit cycle coexist for $m = 0$ and $x_0 = -1.6$ ($I_{ext_2} = 0.45$). The arrows indicate the direction of trajectories. For easier visualization, we plot generalized coordinates (X,Y) corresponding to $(-35x_1 + x_2, 15y_1)$ for seizures (top) and to $(-0.5x_1 + x_2, 0.1y_1)$ for LCs (bottom). The LC is characteristic of RSE. Time series of (b) SLEs and (c) LCs are illustrated. Parameter settings correspond to region VI in Fig. 7.

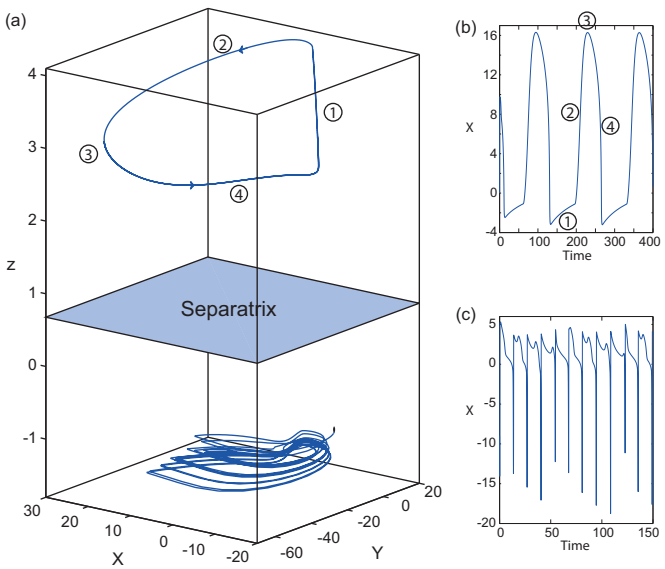

FIG. 4. (Color online) (a) Coexistence of DB and RSE. The simulations are performed without noise. Depolarization block and a stable LC coexist for $m = -8$ and $x_0 = -1.4$ ($I_{ext_2} = 0$). Trajectory segments are numbered in (a) and (b). Depolarization block corresponds to the segment 1 and the normal state to segment 3. The arrows indicate the direction of trajectories. For easier visualization, we plot generalized coordinates (X,Y) corresponding to $(-10x_1 + x_2, 5y_1)$ for DB (top) and to $(-x_1 + x_2, 0.3y_1)$ for the LC (bottom). The LC is characteristic of RSE. Time series of (b) DB and (c) the LC are illustrated. Parameter settings correspond to region V in Fig. 7.

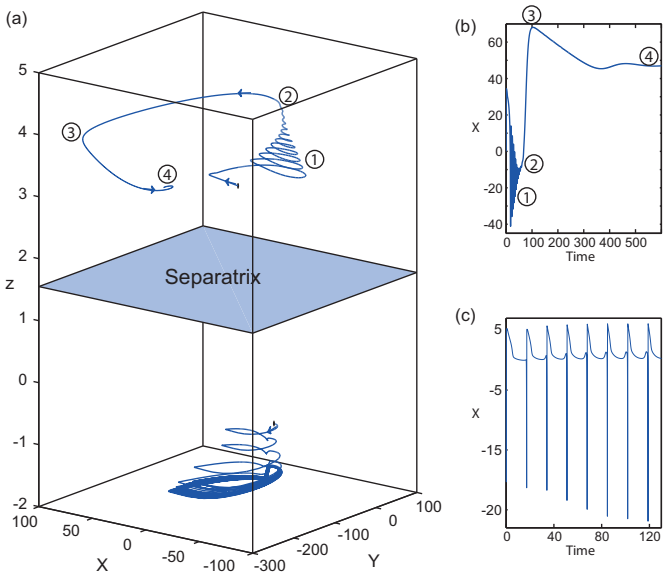

FIG. 5. (Color online) (a) Coexistence of the normal state and RSE. The simulations are performed without noise. The normal state and a stable LC coexist for $m = 0$ ($I_{ext_2} = 0.45$) and $x_0 = -2.1$. Trajectory segments are numbered in (a) and (b). Then following transient seizure-like fast discharges (segment 1), the trajectory evolves towards the normal state (stable fixed point, segment 4), which coexists with the LC. The arrows indicate the direction of trajectories. For easier visualization, we plot generalized coordinates (X,Y) corresponding to $(-35x_1 + x_2, 15y_1)$ for the normal state (top) and to $(-0.5x_1 + x_2, 0.1y_1)$ for the LC (bottom). The LC is characteristic of RSE. Time series of (b) the normal state and (c) the LC are illustrated. Parameter settings correspond to region IX in Fig. 7.

Here we interpret DB with the sufficiently long occupation of the subspace, which contains the trajectory segment 1, in the absence of fast discharges. Figures 4(a) through 4(c) show that the periodic switch of the NS and DB coexists with the LC separated by a saddle periodic orbit. Upon a further change of parameters, with decreasing x_0, the z nullcline is at the Z lower branch (normal state) and the Epileptor stabilizes its stable node, which corresponds to the equilibrium point of the normal state. The NS and LC coexist here and are separated by a saddle periodic orbit [Figs. 5(a) through 5(c)]. Under these conditions, the periodic cycle of offset (normal) and onset (ictal) states breaks and the Epileptor remains in the normal state after a transient epileptiform fast discharge [Figs. 5(a) and 5(b)]. This latter restoration of the normal state following a generalized seizure is more representative of situations under clinical conditions, whereas the cyclic onset and offset of seizure states is more likely found under laboratory conditions [13]. In the following, we will consider the LC as a prime candidate for RSE. We first characterize the LC in more detail and then test its properties experimentally. To locate periodic orbit positions, we use averaging methods [17], which consist in determining the limit cycle averaged curve $\langle x_1 \rangle$ for each z value. The periodic orbits lie on the limit cycle averaged curve and z nullcline intersection. We introduce the slow averaged

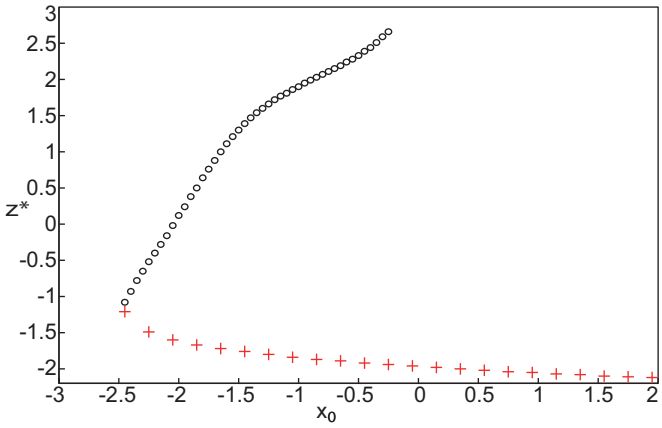

FIG. 6. (Color online) Periodic orbit evolution. Stable (LC) and saddle (separatrix) periodic orbits are labeled as red pluses and black circles, respectively. With decreasing x_0, periodic orbits disappear through a saddle-node-of-periodic-orbit (SNPO) bifurcation.

nullcline [17] as

$$\langle \dot{z} \rangle = 0 = \begin{cases} r[s(\langle x_1 \rangle - x_0) - z - 0.1z^7] & \text{if} \quad z < 0 \\ r[s(\langle x_1 \rangle - x_0) - z] & \text{if} \quad z \geqslant 0, \end{cases}$$

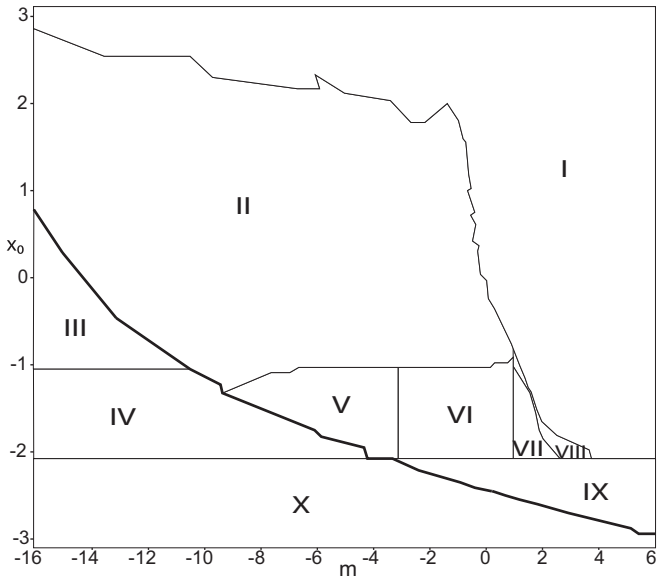

FIG. 7. Parameter space of the fast-slow subsystem with respect to the parameters m and x_0. There are ten regions separated by a boundary (bold line), above which the LC exists, while below it does not. Depolarization block exists for regions II–V. Specifically, in region I only the LC exists (large values of m and x_0). The adjacent area II shows bistability of the LC and DB. In region III only DB exists. Region IV shows a periodic switch of DB and the NS, but no LC exists. Region V presents a periodic switch of DB and the NS and the LC coexists. A SLE occurs via a saddle-node/saddle-node bifurcation pair (region VI) and a saddle-node-homoclinic bifurcation pair (region VII). In region VIII, the homoclinic bifurcation is not completed, thus the equilibrium point of the NS does not exist and only a stable periodic orbit with fast discharges remains, coexisting with the LC. In region IX, normal brain activity in the NS and the LC coexist. In area X, only normal activity in the NS exists.

where the z solutions correspond to periodic orbits. The periodic orbit positions change as x_0 varies. To observe the periodic orbit evolution, we plot the (x_0, z^*) bifurcation diagram (Fig. 6). With decreasing x_0, stable and saddle periodic orbits collide and disappear through a saddle-node-of-periodic-orbit (SNPO) bifurcation. The parameters m and x_0 have a remarkable influence on the fast-slow subsystem dynamics: x_0 leads to a change in the nature of the equilibrium point. For $x_0 = -1.6$, the equilibrium point is a saddle point leading to transitions in the fast-slow subsystem via a saddle-node/saddle-node ($m < 1$) or a saddle-node/homoclinic bifurcation pair ($m \geqslant 1$). Furthermore, the SLE attractor in the upper part of the state space coexists with the LC [Fig. 3(a)],

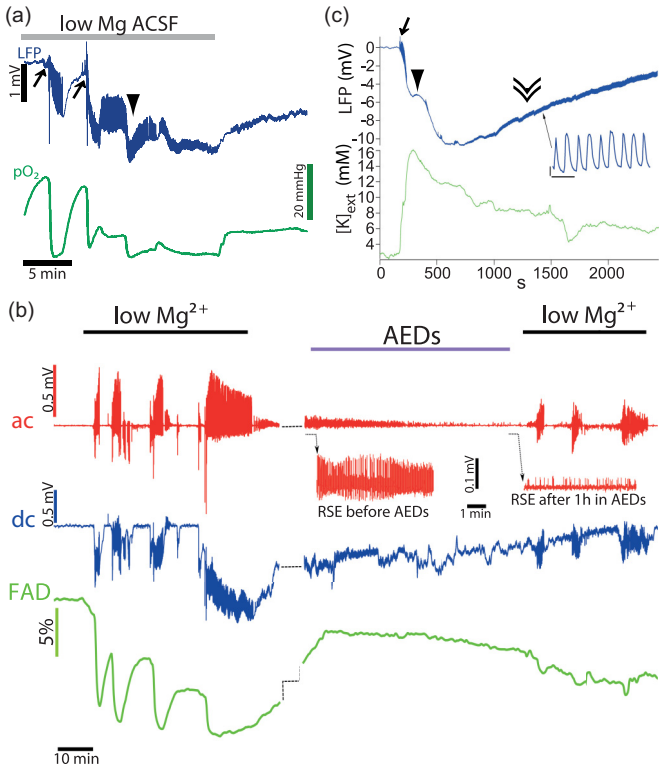

FIG. 8. (Color online) Forcing transitions experimentally. (a) Transition from the SLE to RSE. After two SLEs (arrows) recorded in dc, the system switches to RSE (arrowhead), which persists after removing epileptogenic conditions (end of low Mg^{2+}). Note the persistent dc shift during RSE. Partial oxygen pressure drops considerably during SLEs and does not recover during RSE. Here ACSF denotes artificial cerebrospinal fluid and LFP denotes local field potential. (b) Transition from RSE to the normal state. After three SLEs produced in low Mg^{2+} there is a slow transition SLE to RSE (red top and blue middle traces). The RSE frequency and amplitude could be reduced by simultaneous application of antioxidant, diuretic, and anticonvulsant agents (AEDs). Reinstating the epileptogenic condition (low Mg^{2+}) produced SLEs again. Flavin adenine dinucleotide (FAD) (green bottom trace) is an autofluorescent mitochondrial metabolism cofactor whose fluorescence intensity relates to the tissue oxygen and ATP levels. (c) Transition from the SLE to spreading depression (SD) to RSE. After the SLE (arrow), there is a very large dc shift and considerable accumulation of extracellular K^+ (arrowhead), signaling SD. When the dc shift and K^+ levels recover, the system switches to RSE (double arrow).

which disappears through a SNPO bifurcation (Fig. 6). To characterize the coexisting solutions, we explore the parameter space (m,x_0) of the Epileptor subsystem 1 (Fig. 7) and define ten different areas of coexistence and behavior. The stable equilibrium point of normal brain activity (NS) is found in areas IX and X. As x_0 is decreased, the LC and the saddle periodic orbit disappear through a SNPO bifurcation, which partitions the parameter space into two major segments (bold line in Fig. 7); hence there exists no LC in areas III, IV, and X. Depolarization block is present in region V (periodic switch between DB and the NS and coexistence with the LC), region IV (periodic switch between DB and the NS, but no LC), region III (stable equilibrium point of DB, but no LC), and region II (coexistence of the LC and stable equilibrium point of DB).

Experimental support. From the parameter space in Fig. 7 the Epileptor model predicts that the path between SLEs and RSE requires a large baseline shift as captured by a large change of the z variable, which locks the system in RSE. Experimental testing was performed in postnatal day 7 mice hippocampi. In low Mg^{2+} conditions, SLEs start to occur before evolving into RSE [16]. As predicted, a very large dc shift occurred when the activity switched to RSE [Fig. 8(a)], while a large increase of K^+ and drop of O_2, two possible biophysical contributors to the z variable [13], occurred in the extracellular space [Fig. 8(a)]. Following the model, these levels as well as RSE were maintained after reversing to non-epileptogenic conditions, showing that the hippocampus was locked in a RSE regime, which may explain why RSE is very difficult to treat in the clinic. However, the model predicts that there exists a path back to normal activity (area IX). We reasoned that two biophysical parameters may maintain a low-z value: a large production of reactive oxygen species [18] and a change in GABAergic function [19]. Using a combination of a detoxifying agent (to remove reactive oxygen species), a diuretic (to restore GABAergic function), and a common antiepileptic drug (AED) Fig. 8(b), we reversed the activity back to a normal regime [Fig. 8(b); see the insets of RSE before AEDs and RSE after AEDs]. As predicted, the dc shift and O_2 level were partially recovered, in effect bringing z back. Reinstating epileptogenic conditions, we could trigger SLEs again, showing that we succeeded in bringing the hippocampus to a normal regime. The model also predicts the existence of different paths between SLEs, DB, the normal state, and RSE. Experimentally, spreading depression onset occurs when extracellular K^+ reaches a 10–12 mM threshold value [20]. In addition, although the dc shift only reaches 1–2 mV during SLEs, it reaches 10 mV during spreading depression, i.e., when neurons go into DB [20]. In some instances, we found that SLEs evolved into DB and then into RSE [Fig. 8(c)]. In keeping with the expected behavior of the z variable, the steady increase of extracellular K^+ above 10 mM allows the transition to DB (with a corresponding dc shift greater than 10 mV). As the system recovers and extracellular K^+ decreases, another transition occurs to RSE, in which the system remains locked.

Both theoretical and experimental approaches demonstrate that SLEs, RSE, and DB belong to the normal repertoire of brain activities, as we could force the hippocampus to navigate through several regions of the state space as suggested by the Epileptor. It is far from trivial to interpret the parameters and variables in the phenomenological Epileptor model. Nevertheless, some correspondences suggest themselves, such as the interpretation of x_0 to be linked to epileptogenicity [15] or the permittivity variable z to be involved in energy consumption. On this basis, the parameter manipulations in the experiments resulted in dynamic changes of the discharges in full consistency with the parameter space as summarized in Fig. 7. Importantly, together the attractor structure in state space and the parameter space of the Epileptor predict where and how to act to escape pathological states to return to normal activity. Based on these theoretical predictions, we could demonstrate for how to escape RSE, which bears considerable translational value. Our approach proposed here towards the understanding of pathological and physiological states can be now systematically extended through detailed experimental paradigms for the validation of the various paths in the predicted parameter space.

[1] A. A. Leo, J. Neurophysiol. **7**, 359 (1944).
[2] H. Kager, W. Wadman, and G. Somjen, J. Neurophysiol. **84**, 495 (2000).
[3] J. R. Cressman, Jr., G. Ullah, J. Ziburkus, S. J. Schiff, and E. Barreto, J. Comput. Neurosci. **26**, 159 (2009).
[4] G. P. Krishnan and M. Bazhenov, J. Neurosci. **31**, 8870 (2011).
[5] E. Barreto and J. R. Cressman, J. Biol. Phys. **37**, 361 (2011).
[6] S. A. Mayer, J. Claassen, J. Lokin, F. Mendelsohn, L. J. Dennis, and B.-F. Fitzsimmons, Arch. Neurol. **59**, 205 (2002).
[7] D. Pietrobon and M. A. Moskowitz, Nat. Rev. Neurosci. **15**, 379 (2014).
[8] M. A. Rogawski, Arch. Neurol. **65**, 709 (2008).
[9] J. Ziburkus, J. R. Cressman, E. Barreto, and S. J. Schiff, J. Neurophysiol. **95**, 3948 (2006).
[10] F. Wendling, F. Bartolomei, J. Bellanger, and P. Chauvel, Eur. J. Neurosci. **15**, 1499 (2002).
[11] S. N. Kalitzin, D. N. Velis, and F. H. Lopes da Silva, Epilepsy Behav. **17**, 310 (2010).
[12] P. Touboul, J. Valbousquet, I. Pourrat-Vanoni, M.-F. Alquier, D. Benchimol, and C. Pradier, Santé Publique **23**, 385 (2011).
[13] V. K. Jirsa, W. C. Stacey, P. P. Quilichini, A. I. Ivanov, and C. Bernard, Brain **137**, 2210 (2014).
[14] G. B. Ermentrout and D. H. Terman, *Mathematical Foundations of Neuroscience* (Springer, Berlin, 2010), Vol. 35.
[15] T. Proix, F. Bartolomei, P. Chauvel, C. Bernard, and V. K. Jirsa, J. Neurosci. **34**, 15009 (2014).
[16] P. P. Quilichini, D. Diabira, C. Chiron, Y. Ben-Ari, and H. Gozlan, Eur. J. Neurosci. **16**, 850 (2002).
[17] A. Shilnikov and M. Kolomiets, Int. J. Bifurcat. Chaos **18**, 2141 (2008).
[18] A. J. Kowaltowski, N. C. de Souza-Pinto, R. F. Castilho, and A. E. Vercesi, Free Radical Biol. Med. **47**, 333 (2009).
[19] V. I. Dzhala, K. V. Kuchibhotla, J. C. Glykys, K. T. Kahle, W. B. Swiercz, G. Feng, T. Kuner, G. J. Augustine, B. J. Bacskai, and K. J. Staley, J. Neurosci. **30**, 11745 (2010).
[20] T. Gloveli, D. Albrecht, and U. Heinemann, Dev. Brain Res. **87**, 145 (1995).